Springer

KSME

Journal of Mechanical Science and Technology 32 (2) (2018) 781~791
www.springerlink.com/content/1738-494x(Print)/1976-3824(Online)
DOI 10.1007/s12206-018-0126-0

Parameter analysis and design for the hovering thrust of a quad-rotor air vehicle using CFD and design of experiment †

Jaehyun Yoon and Jongsoo Lee*

School of Mechanical Engineering, Yonsei University, Seoul 120-749, Korea

(Manuscript Received August 10, 2017; Revised October 30, 2017; Accepted October 30, 2017)

Abstract

The present study explores the aerodynamic parameter analysis and design of a quad-rotor air vehicle in hover using Computational fluid dynamics (CFD) and Design of experiments (DOE). Following the identification of the center distance between rotors in terms of hovering thrust and velocity/pressure distributions, the blade-shape parameter design is implemented to predict the optimal levels of twist angle, maximum chord position, blade cross-section type and twist position, and the significant factor effects and factor interactions in DOE are discussed. The present study shows that optimized twist angle and twist-starting position enables maximum hovering thrust in the proposed quad-copter.

Keywords: Quad-rotor air vehicle (Quad-Copter); Computational fluid dynamics; Hovering thrust; Center distance; Blade-shape parameters; Design of experiment

1. Introduction

A quad-copter has a simpler structure than that of a helicopter, which is a conventional rotorcraft, and has the advantages of vertical take-off and landing, and flexible maneuverability. By controlling the propellers with four rotors, a quad-copter can fly forward/backward and left/right, and is currently suitable for unmanned airplanes [1].

The maximum aerodynamic performance of a quad-copter is gained from low fuel consumption; therefore, its small size and light weight are important. To increase aerodynamic performance, it can be useful to change the shape of the blade in a way that does not affect the size or weight of the air vehicle [2, 3]. A multi-rotor air vehicle for use as a flying robot has been studied in the context of aerodynamics, dynamics, and control for performance, stability and maneuverability [4-6].

Flow interference is expected between each rotor of a quad-copter, because all four propellers rotate simultaneously. In previous studies, it was revealed through Computational fluid dynamics (CFD) and actual experiments that changes in the drag and lift coefficients have effects that are dependent upon the distances between the rotors. A two-dimensional numerical simulation of cross-flow around four cylinders in an in-line rectangular configuration has been studied using the lattice Boltzmann method [7]. The lift force of a quad rotor helicopter has been explored by changing the distance size between rotors [8].

The present study explores the aerodynamic parameter analysis and design of a quad-rotor air vehicle in hover based on Computational fluid dynamics (CFD) and Design of experiments (DOE). In a quad-copter consisting of four rotors, flow interference is expected in the areas between rotors. To confirm this expectation, we analyzed the effect of the Center distance (CD) between rotors to identify the flow interference in term of flow stability.

The present study includes a numerical study based on the Computational fluid dynamics (CFD) of the blade motion and hovering thrust of a multi-rotor air vehicle (Quad-copter). CFD analysis data based on the proposed quad-copter model was used to numerically explore variables such as twist angle, maximum chord position, blade cross-section type, and twist position using ANSYS-FLUENT, a commercial software package that calculates computational fluid dynamics. This paper discusses the mathematical modeling and numerical simulation of the hovering thrust of a quad-copter by evaluating the velocity and pressure distributions around the rotors. Based on a number of CFD results, a method of Analysis of means (ANOM) is performed in order to facilitate parameter design, predict optimum parameter levels, identify parameter effects, and estimate the relative contribution of each parameter to hovering thrust in the context of Design of experiments (DOE).

*Corresponding author. Tel.: +82 2 2123 4474, Fax.: +82 2 362 2736
E-mail address: jleej@yonsei.ac.kr
† Recommended by Associate Editor Chang-Wan Kim

Table 1. Weight estimation of proposed quad-copter.

Part	Weight [g]	Quantities	Total weight [g]
Body	411	1	411
Blade	12	4	48
Motor	27	4	108
Battery	100	1	100
Board	17	1	17
Transmission	7	4	28
Receiver	10	1	10
Other parts	150	-	150
Total	-	-	872

Fig. 1. Proposed quad-copter model.

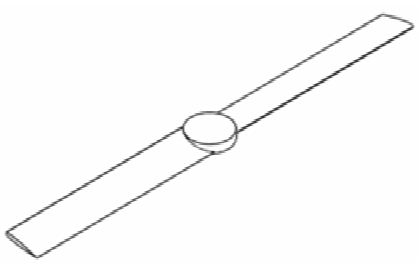

Fig. 2. Rectangular blade with NACA0012 airfoil.

2. Quad-copter model

The proposed model of a quad-rotor air vehicle (Quad-copter) is shown in Fig. 1. The total weight of the quad-copter and its components are evaluated prior to the computation of the quad-copter's aerodynamic performance in hover. The material used for the major parts of the quad-copter is assumed to be carbon fiber. Including blades, motors, batteries, circuit board, transmission and receiver, the minimum weight of the proposed quad-copter is approximately 872 g, as shown in Table 1. With the addition of other important parts such as GPS and camera equipment to address side wind/air-load effects and weather conditions, this flying vehicle is quantitatively estimated to be heavier than the minimum weight of 872 g.

Table 2. Parameters of rectangular blade.

Parameter	Value	Unit
Airfoil	NACA0012	-
Chord (c)	0.02	m
Angle of attack (α)	10	degree
Radius (R)	0.12	m
# of blades	2	-

Since the present study focuses on thrust performance in hover, an analytical expression of thrust force is briefly discussed using a rectangular blade, and its parameter values are shown in Fig. 2 and Table 2. From the Blade element theory (BET), the thrust is obtained as follows [4, 9]:

$$T = \frac{1}{2} b \rho \int_r^R V_r^2 c C_L dr. \tag{1}$$

The induced velocity is calculated in terms of the rotational speed to the radial direction as follows:

$$V_r = \Omega r. \tag{2}$$

The lift coefficient is simplified as:

$$C_L = 2\pi\alpha. \tag{3}$$

For a single rotor, a hovering thrust value of 2.6319 N was calculated with a rotational speed of Ω = 5200 rpm; blade parameter values are listed in Table 2. According to the blade element theory, a thrust force of 2.6319 N per rotor could be applied to the proposed quad-copter with a minimum weight of approximately 872 g.

3. Computational fluid dynamics analysis

3.1 Flow equations

Consider the Reynolds number as follows [10]:

$$\mathrm{Re} = \frac{\rho c U}{\mu} \tag{4}$$

where the air density and viscosity are ρ = 1.225 kg/m^3 and μ = 1.745E-05 kg/ms, respectively. The chord length, c = 0.02 m, is selected as shown in Table 2.

When the rotational speed exceeds Ω = 5200 rpm, the Reynolds number is Re $\geq$ 5000, implying that the flow phenomenon is turbulent. Since the Re decreases near the center of the blade, its values from the laminar region to the turbulence region are included. Accordingly, the Spalart-Allmaras model [11] was used in the present study. This model accommodates a turbulence in which the closest gap to a wall is applied and also facilitates flow analysis of the laminar, turbu-

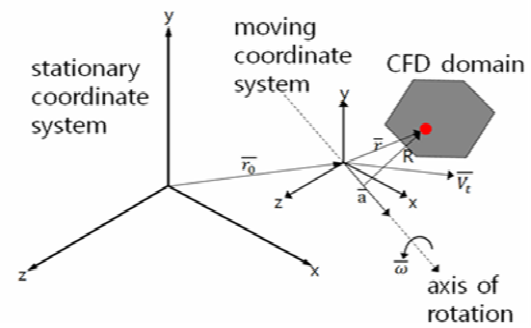

Fig. 3. Moving reference frame [10].

lence, and transition zones.

Fig. 3 shows the fixed and rotational coordinates of a component rotating with rotational speed. Consider a coordinate system that is translating with linear velocity and rotating with angular velocity relative to a stationary (Inertial) reference frame, as illustrated in Fig. 3 (Moving reference frame). The origin of the moving system is located by a position vector. The computational domain for the CFD problem is defined with respect to the moving frame such that an arbitrary point in the CFD domain can be located by a position vector from the origin of the moving frame. The fluid velocities can be transferred from the stationary frame to the moving frame using the following relationships [12]:

$$\vec{v}_r = \vec{v} - \vec{u}_r \tag{5}$$

$$\vec{u}_r = \vec{V}_t + \vec{\omega} \times \vec{r}. \tag{6}$$

In the above equations the relative velocity (The velocity viewed from the moving frame), the absolute velocity (The velocity viewed from the stationary frame), is the velocity of the moving frame relative to the inertial reference frame, the translational frame velocity. It should be noted that both angular velocity and linear velocity can be functions of time.

The Navier-Stokes equations for 3-dimensional transient incompressible viscous flow can be expressed as follows [13-16]:

$$\frac{\partial \rho}{\partial t} + \nabla \cdot \rho \vec{v}_r = 0 \tag{7}$$

$$\frac{\partial}{\partial t}(\rho \vec{v}_r) + \nabla \cdot (\rho \vec{v}_r \vec{v}_r) + \rho(2\vec{\omega} \times \vec{v}_r + \vec{\omega} \times \vec{\omega} \times \vec{r} + \vec{\alpha} \times \vec{r} + \vec{a}) =$$
$$-\nabla p + \nabla \cdot \bar{\bar{\tau}}_r + \vec{F} \tag{8}$$

$$\frac{\partial}{\partial t}(\rho E_r) + \nabla \cdot (\rho \vec{v}_r H_r) = \nabla (k \nabla T + \bar{\bar{\tau}}_r \cdot \vec{v}_r) + S_h. \tag{9}$$

Eqs. (7)-(9) are the continuity equation, momentum equation, and energy equation, respectively. $\vec{\alpha}$ and $\vec{a}$ in the momentum equation can be expressed as follows:

$$\vec{\alpha} = \frac{d\vec{\omega}}{dt} \tag{10}$$

$$\vec{a} = \frac{d\vec{v}_t}{dt}. \tag{11}$$

However, the energy equation is not included in an incompressible flow analysis, since the effect on heat is negligible. With the assumption that the air density is constant, the continuity and momentum equations for incompressibility can be expressed as follows:

$$\rho \cdot \nabla \vec{v}_r = 0 \tag{12}$$

$$\rho \frac{\partial \vec{v}_r}{\partial t} + \rho \vec{v}_r \cdot \nabla \vec{v}_r + \rho(2\vec{\omega} \times \vec{v}_r + \vec{\omega} \times \vec{\omega} \times \vec{r} + \vec{\alpha} \times \vec{r} + \vec{a}) =$$
$$-\nabla p + \nabla \cdot \bar{\bar{\tau}}_r + \vec{F}. \tag{13}$$

3.2 Computational modeling

The computational fluid dynamic analysis of a quad-copter in flight is conducted using ANSYS-FLUENT [12], where moving reference frame techniques are adopted to accommodate the physics of blade rotation. The flow analysis domain for the air vehicle and the rotating domain for the rotor blades are shown in Fig. 4. The size of the flow analysis domain is set to 10 times the distance between rotors in order to identify the flow phenomena between and around the rotors and blades. A cylindrical-type rotating domain is generated for the rotating motion of a rotor blade [3, 12].

As shown in Fig. 4(a), the no-slip inlet condition was applied to the upper part of the cube to allow fluid to flow in. Additionally, the no-slip outlet condition was applied to the remaining five sides so that the fluid flowing in can flow out again. The shape in Fig. 4(b) was modeled as a cylinder to depict the rotation of the blade; the mesh motion condition, which does not share a node with the flow field, was applied. Because the flow field and the cylinder depicting rotation do not share nodes with one another, the shape of the cylinder also exists inside the flow field. On the surface of the cylindrical shape, inside the flow field in Fig. 4(a) and the cylinder surface in Fig. 4(b), an interface condition is applied so that the data of the flows can be exchanged with each other. A rigid body was represented by constructing walls on the shape surface of the four blades.

All of the meshes were generated as tetra meshes. To confirm the flows and pressure distribution around the blade, the rotation zone was set with an element size of 10^{-2} m. To confirm the change in pressure, the blade surface was finely generated with an element size of 10^{-3} m. The number of generated nodes in the four rotation zones (Cylinders) for all shapes was 82000 to 83000 depending on blade shape. Because the mesh of the flow field has less influence on the flow when it is further away from the rotation zone, the element size was set to gradually increase further from the rotation zone. 83000 nodes were generated.

The calculation was performed with a time step size of 0.0001442308 (4.5°) and the convergence values for the con-

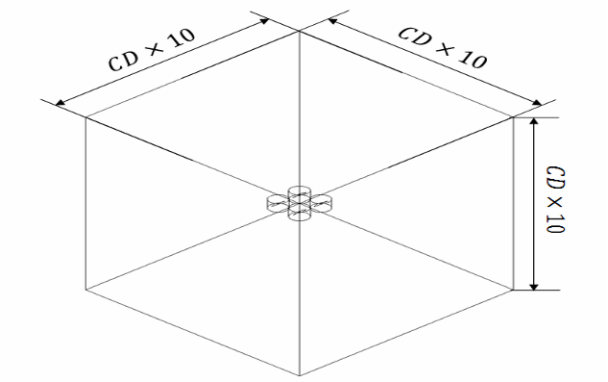

(a) Fluid domain

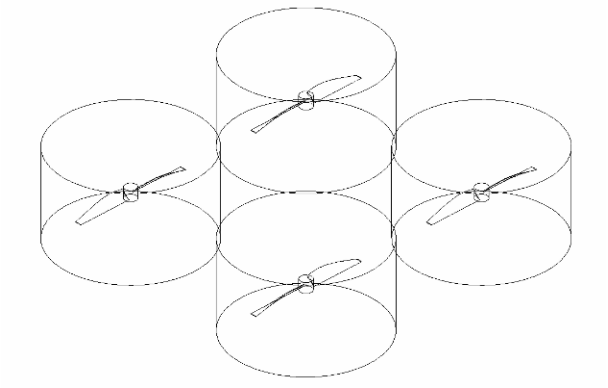

(b) Rotor domain

Fig. 4. CFD analysis domain.

tinuity, X-, Y- and Z- velocities were set at 10^{-3}. Because there are four blades that rotate in an abnormal state, many calculations are required for convergence. To reach convergence values, the number of time steps was set equal to 16000 (200 cycles).

4. Effect of center distance

The present study defines the distance between rotors as the Center distance (CD) in order to identify the flow interference and instability between rotors, as shown in Fig. 5.

In this study, prior to the parameter design of the detailed blade shape, we first identified the flow effects that were interfering with each other as a function of the distances between the four rotors of the quad-copter. The rectangular blade shown in Fig. 2 was used to observe the mutual interference effect based on the change in distance between rotors. Analysis was carried out for the four blades by selecting distances between rotors of CD = 300, 400 and 500 mm, and rotational speeds of Ω = 5200 and 6000 rpm.

Using ANSYS-FLUENT, the thrust value of the four rotors was calculated. The equation that calculates the thrust from the CFD analysis is as follows:

$$T = \iint \rho \vec{V}(r,\psi) ds \vec{V}(r,\psi) . \tag{14}$$

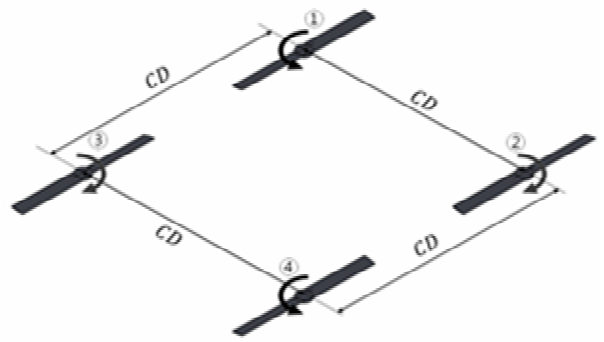

Fig. 5. Center distance (CD) between rotors with rotational direction.

The above thrust equation depicts the relationship of this angle as a function of the radial and rotational directions and can be expressed with the mass flow and velocity vector, depending on the rotation, as follows:

$$T = \dot{m}\left|\vec{V}\right| . \tag{15}$$

The equations for mass flow and velocity vector depending on the blade's radial and rotational directions can be expressed as follows:

$$\dot{m} = \iint \rho \vec{V}\left(r,\psi\right) r dr d\psi \tag{16}$$

$$\left|\vec{V}\right| = \frac{1}{R_1 - R_0}\int_{R_0}^{R_1} \vec{V}\left(r\right) dr . \tag{17}$$

To evaluate the CFD results, a comparison was made with the thrust value obtained from the BET of Eqs. (1)-(3) by calculating a single rotor only with the blade shape shown in Fig. 2.

The thrust values generated on each of the four rotors are summarized in Table 3, wherein the mean and Standard deviation (SD) of 4 hovering rotors are presented. When the center distance between rotors is CD = 300 mm, the thrust values of each rotor are not identical and the standard deviation is at the highest value of SD = 0.0942. When the center distance is CD = 400 mm and rotational speed is Ω = 5200 rpm, the thrust values generated from 4 rotors were turned out to be constant. The data obtained through CFD exhibited an average thrust value of 2.6908 N, showing that the two values of CFD and 'BET-Single rotor = 2.6319 N' agree well. Additionally, when the center distance is CD = 500 mm, the thrust values at each rotor again begin to differ and the average thrust is reduced. For Ω = 6100 rpm, the average value of thrust for each center distance differs significantly from that obtained from 'BET-Single rotor', since the blade element theory could not capture the complex flow interference among rotors as the rotating speed increases. For a total of 6 calculations, the thrust value with CD = 400 mm and Ω = 5200 rpm is the most consistent in terms of standard deviation (SD = 0.0091), as shown in Table 3.

Table 3. Calculation results of hovering thrust.

Rotational speed [rpm]	Center distance [mm]	Rotor ID	Thrust (CFD) [N]	Mean SD [N]	Thrust (BET-single rotor) [N]
5200	300	1	2.6319	2.7699 0.0942	2.6319 (Single rotor)
		2	2.7946		
		3	2.8437		
		4	2.8092		
	400	1	2.6872	2.6908 0.0091	
		2	2.6798		
		3	2.6966		
		4	2.6998		
	500	1	2.6427	2.6639 0.0170	
		2	2.6575		
		3	2.6782		
		4	2.6771		
6000	300	1	3.9650	3.9391 0.0249	3.5040 (Single rotor)
		2	3.9216		
		3	3.9554		
		4	3.9143		
	400	1	3.7233	3.7184 0.0107	
		2	3.7077		
		3	3.7116		
		4	3.7309		
	500	1	3.7571	3.7751 0.0154	
		2	3.7679		
		3	3.7846		
		4	3.7909		

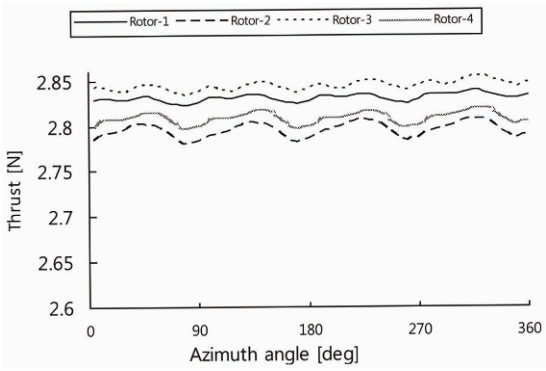

(a) Thrust performance (CD = 300 mm)

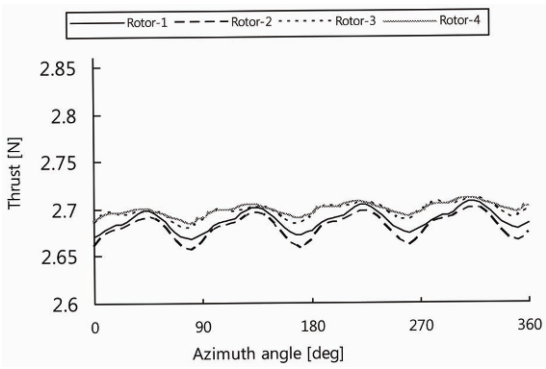

(b) Thrust performance (CD = 400 mm)

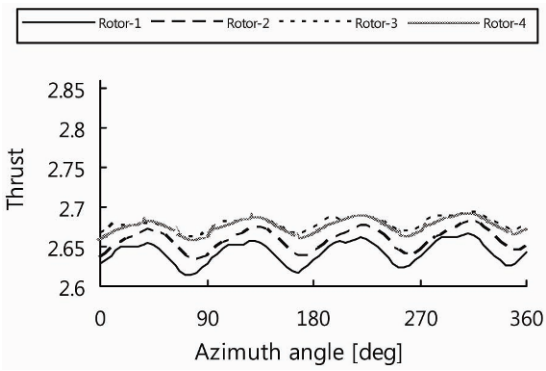

(c) Thrust performance (CD = 500 mm)

Fig. 6. Thrust with respect to center distance (Ω = 5200 rpm).

Examining the thrust values in the one-cycle thrust graph in Fig. 6, it is found that the case of CD = 400 mm exhibits the smallest thrust deviations among 4 rotors; the cases of the narrower distance (CD = 300 mm) and wider distance (CD = 500 mm) present inconsistent thrust patterns due to the presence of flow interference. Fig. 7 shows a velocity distribution represented by only two rotors (Actually, all four rotors are placed in a symmetrical relation). As shown in the velocity distribution result, the flow is stabilized for the 400 mm distance, and the flows are symmetric for both sides. The pressure distribution for only two rotors, similar to the velocity distribution, is shown in Fig. 8. In the pressure distribution of the CD = 300 mm (Fig. 8(a)), the pressure value gets increased since the distance between two blade tips is gets close. For CD = 400 mm and 500 mm, the pressure distributions of the slipstream on both sides are relatively equal, similar to the velocity distribution.

From results in Table 3 and Figs. 6-8, the present study supports that the smallest center distance (CD = 300 mm) generates the largest thrust value (Mean = 2.7699 N) due to the closeness of 4 rotors while the thrust variation is the largest (SD = 0.0942 N) due to the flow interference. For the case of CD = 500 mm, the average value of 4-rotor thrusts is smaller than the case of CD = 400 mm due to the apartness in the center distance. Based on such results, the center distance of CD = 400 mm is finally selected for the further analysis and blade-shape parameter design of the quad-copter in this study.

5. Effect of blade-shape parameters

5.1 Blade-shape configuration

After evaluating the interference effect between rotors, a number of blade-shape parameters were varied based on the fixed value of the center distance, CD = 400 mm. It is assumed that the interaction between CD and blade-shape pa-

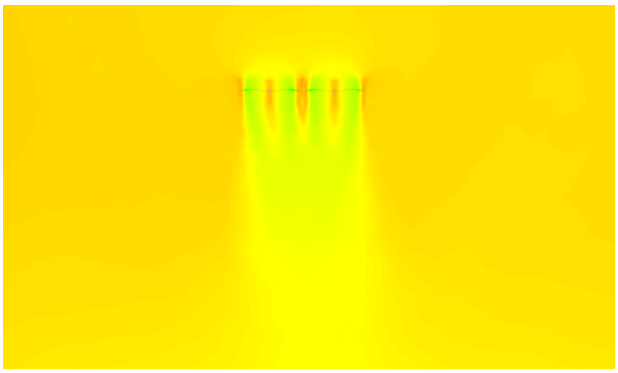

(a) Velocity distribution (CD = 300 mm)

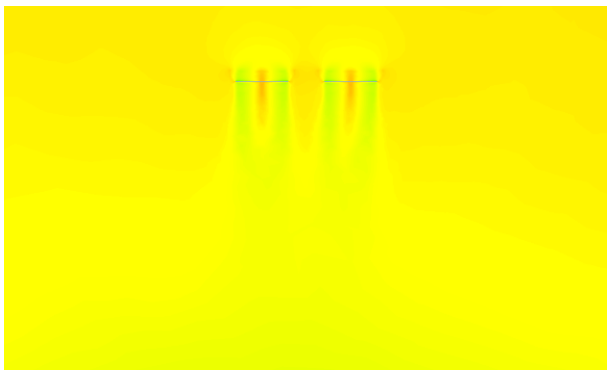

(b) Velocity distribution (CD = 400 mm)

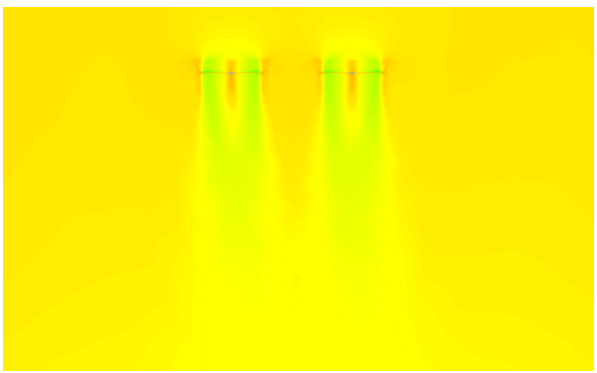

(c) Velocity distribution (CD = 500 mm)

Fig. 7. Velocity distributions with respect to center distance (Ω = 5200 rpm).

rameters is neglected in the present study. A total of 4 shape parameters such as twist angle, maximum chord-tapering position, type of airfoil cross-sectional shape, and starting position of a twist are selected as shown in Table 4, wherein the four factors of blade-shape parameter have three levels of discrete numerical values in the context of Design of experiments (DOE).

The twist angle is selected in three levels from 10° to 30° at 10° intervals. The change in the chord length, referred to as taper shape, is defined. For the maximum chord length (0.025 m), the blade is modeled to have a maximum chord length at 20 %, 30 % and 40 % of the position of the blade length. For the cross-section of the blade, symmetric (Upper/lower cambers are changed symmetrically) and asymmetric (Upper/lower cambers are changed asymmetrically) shapes are employed as shown in Fig. 9. For the twist position, three values are selected such that a twist angle begins at 0 %, 20 % and 40 % of the position of the blade length.

Table 4. Four factors and their three levels of blade shape parameter.

	A Twist angle [deg]	B Max. chord position	C Section type	D Twist position
Level-1	10	r/R = 20 %	Symmetric	r/R = 0 %
Level-2	30	r/R = 30 %	NACA0012	r/R = 20 %
Level-3	50	r/R = 40 %	Asymmetric	r/R = 40 %

(a) Pressure distribution (CD = 300 mm)

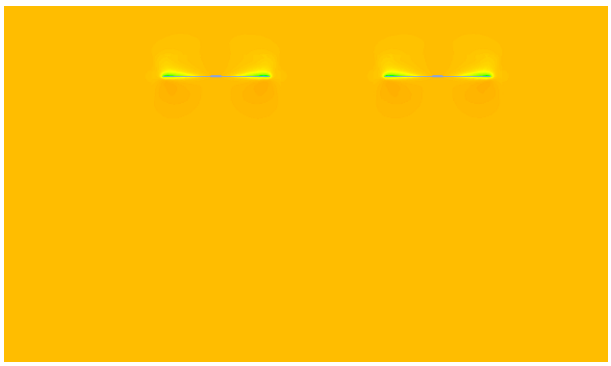

(b) Pressure distribution (CD = 400 mm)

(c) Pressure distribution (CD = 500 mm)

Fig. 8. Pressure distributions with respect to center distance (Ω = 5200 rpm).

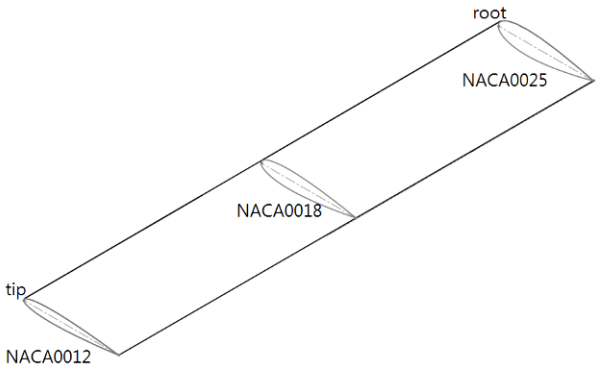

(a) Symmetric cross-section

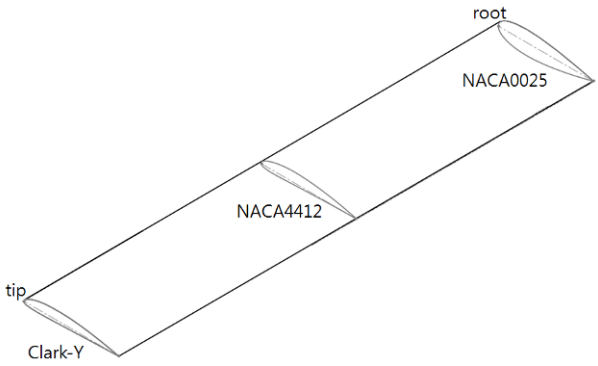

(b) Asymmetric cross-section

Fig. 9. Span-wise variation of airfoil section.

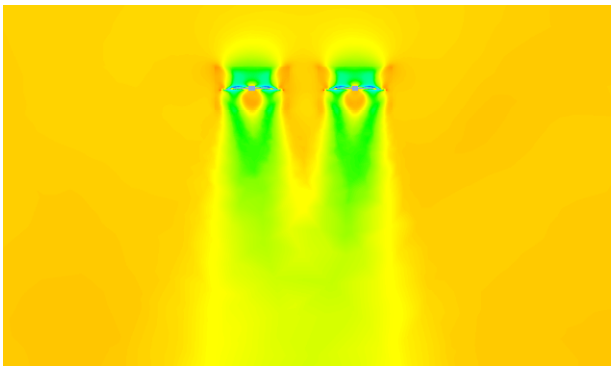

(a) Velocity distribution

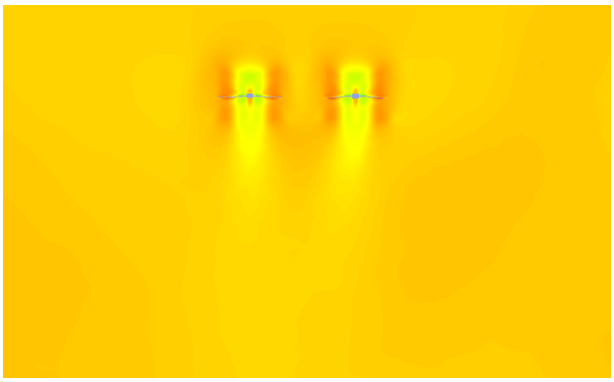

(b) Pressure distribution

Fig. 10. Velocity & pressure distributions for maximum thrust (DOE #8 in Table 5).

5.2 Flow analysis results

In this study, an Orthogonal array (OA) table that allows the fewest number of numerical experiments is used. A CFD-based flow analysis is conducted using the orthogonal array data shown in Table 4. For the four-factor, three-level orthogonal array table, the main effects of each factor are confirmed, but interactions between factors are not taken into account [17].

To evaluate the hovering thrust according to the change in blade-shape parameters, a total of 9 CFD-based flow analyses were conducted using orthogonal array in the context of DOE. It is noted that fixed values of the center distance, CD = 400 mm, and the rotating speed, Ω = 5200 rpm, are used. The CFD-based hovering thrust under the change in blade shape parameters is summarized in Table 5, wherein each rotor generates relatively similar thrust values for all 9 DOE data. It is implied that a fixed center distance of CD = 400 mm provides stability in hovering thrust, and these results are compatible with those presented in Table 3.

From 9 CFD results, the lowest thrust value was exhibited by the blade shape with a constant cross section with no cross-sectional change, a 30° angle from the starting position of the blade to the 20 % position in the length direction, a twist where the angle from the 20 % position of the length direction to the end becomes 0°, and the maximum chord length at the 20 % position in blade length. Conversely, the largest thrust value was exhibited by the blade shape with a symmetrical cross-sectional change, a 50° angle from the starting position of the blade to the 40 % position in the length direction, a twist where the angle from the 40 % position in the length direction to the end becomes 0°, and the maximum chord length at the 20 % position in the blade length direction.

Pressure and velocity distributions for maximum thrust (DOE #8 in Table 5) and minimum thrust (DOE #6 in Table 5) are shown in Figs. 10 and 11, respectively. The high downwash velocity in Fig. 10(a) generates the high pressure difference between upper and lower rotor surface in Fig. 10(b), thereby resulting in the maximum thrust in DOE #8.

In Fig. 10, the pressure distribution appears evenly from the starting portion of the blade to the end. The starting part of the blade has a low induced velocity and pressure is produced by the large angle of attack. The angle of attack becomes smaller closer to the end of the blade, thereby reducing drag. It appears that superior thrust is exhibited, and the flow at the upper side of the blade moves quickly toward the asymmetrical cross section, thereby producing pressure and improved thrust performance.

In contrast, the results of DOE #6 in Fig. 11, which had the lowest thrust performance, show no difference in speed and/or pressure in the velocity and/or pressure distributions. It seems that a low thrust was generated since a difference in pressure could not be produced due to the small angle of attack and

Table 5. CFD based thrust calculation in orthogonal array table.

Run #	A	B	C	D	Rotor-1 [N]	Rotor-2 [N]	Rotor-3 [N]	Rotor-4 [N]	Average [N]
1	1	1	1	1	0.3121	0.2205	0.3338	0.3449	0.3028
2	1	2	2	2	0.4723	0.4776	0.4864	0.4907	0.4817
3	1	3	3	3	2.9118	2.9450	2.9381	2.9496	2.9396
4	2	1	2	3	7.4032	7.3972	7.3285	7.3592	7.3720
5	2	2	3	1	2.0944	2.1163	2.0871	2.0963	2.0985
6	2	3	1	2	0.0323	0.0335	0.0709	0.0444	0.0453
7	3	1	3	2	10.5886	10.5128	10.2846	10.4163	10.4506
8	3	2	1	3	15.3263	15.3797	15.2389	15.2823	15.3068
9	3	3	2	1	9.9915	10.0518	9.9356	9.8896	9.9671

(a) Velocity distribution

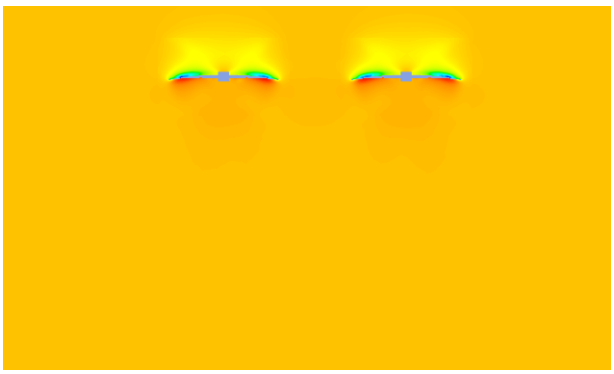

(b) Pressure distribution

Fig. 11. Velocity & pressure distributions for minimum thrust (DOE #6 in Table 5).

symmetrical cross-sectional shape.

5.3 DOE-based parameter design

A parameter design is conducted using a Design of experiments (DOE) method [17]. These are expressed using four-factor, three-level orthogonal arrays (Table 4). In this study, the thrust performance as a function of the shape of the quad-copter blade was examined. The Analysis of means (ANOM) was used to identify the effects of each factor through OA in the context of DOE. The ANOM is a technique that analyzes a given system by obtaining the average value of a response function for each level of the design variables. It can be used to determine major factors, derive the optimal level combination of factors, and identify trends in a system.

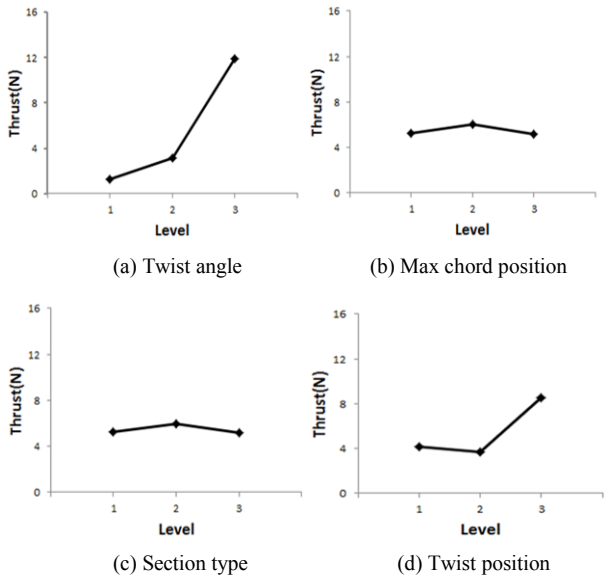

Fig. 12. Factor effects.

Using orthogonal array CFD analysis data as shown in Table 5, the results of the factor effects obtained from ANOM are presented in Fig. 12 and Table 6. In terms of the orthogonal arrays, the optimal parameter levels are predicted to be [A-3 / B-2 / C-2 / D-3], which are similar to those of DOE #8 in Table 5. In Fig. 12, among the factors affecting the thrust performance of the quad-copter, the twist angle (Factor A) and the starting position of the twist position (Factor D) were found to have large effects. Alternatively, the effects of the maximum chord length (Factor B) and cross-section type (Factor C) were confirmed to be relatively small.

The design result is obtained from the orthogonal-array-based ANOM, which uses a small number of design data compared to the full factorial design. Such insufficient data information would not reflect interactions between factors;

Table 6. Factor effects for maximum hovering thrust.

Factor	Level	Thrust [N]
A: Twist angle	1	1.2414
	2	3.1718
	3	11.9082
B: Max. chord position	1	5.2183
	2	5.9403
	3	5.1627
C: Section type	1	5.2183
	2	5.9403
	3	5.1627
D: Twist position	1	4.1226
	2	3.6592
	3	8.5395

thus, we now examine factor interactions based on twist angle (Factor A) as shown in Fig. 13. Figs. 13(a) and (b) show factor interactions of the maximum chord length position and cross-sectional shape with twist angle, respectively; they seem to have large interactions with twist angle with respect to the thrust performance. For the section type (Factor C) shown in Fig. 13(c), there was no effect on the thrust performance.

The general form of the predictive equation is as follows [17]:

$$\bar{d}_{predictive} = \bar{d}_{overall} + (\bar{d}_A - \bar{d}_{overall}) + (\bar{d}_B - \bar{d}_{overall}) + (\bar{d}_C - \bar{d}_{overall}) + (\bar{d}_D - \bar{d}_{overall}) \quad (18)$$

where $\bar{d}_{overall}$ is the overall average response of the thrust for the entire orthogonal array and $\bar{d}_A, \bar{d}_B, \bar{d}_C, \bar{d}_D$ are the response averages for factors A, B, C and D, respectively. The factor values corresponding to the factor levels obtained from ANOM are used in the predictive equation in order to identify the optimum thrust response. In our study, $\bar{d}_{overall}$ = 5.4404 using the factor effect values in Table 6, is. By substituting parameter values of $\bar{d}_A$ = 11.9082 (A-3), $\bar{d}_B$ = 5.9403 (B-2), $\bar{d}_C$ = 5.9403 (C-2) and $\bar{d}_D$ = 8.5395 (D-3) into Eq. (18), the corresponding thrust response is predicted to be $\bar{d}_{predictive}$ = 16.0069.

The predictive equation is now employed in order to derive the optimal level of factor combination through ANOM. Prior to the DOE-based optimization, the best in DOE is [A-3 / B-1 or B-2 / C-1 / D-3], which exhibited the highest thrust in Table 5. To derive the optimal level combination using ANOM, a predictive equation was used. Table 7 summarizes the highest thrust performance values in terms of best in DOE, ANOM-based predictive design, and its actual CFD value. The optimal factor levels were calculated with A-3, B-2, C-2 and D-3. The optimal shape obtained through the predictive equation was validated through CFD, and the thrust values were confirmed to be similar using the predictive equation. Fig. 14 compared

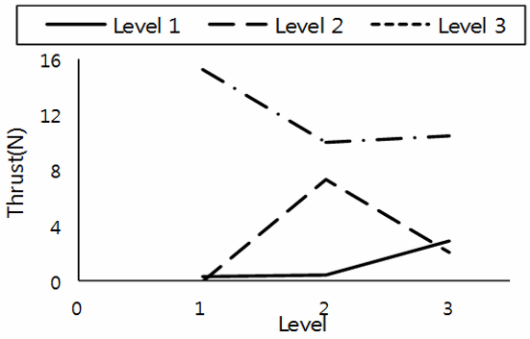

(a) Max. chord position

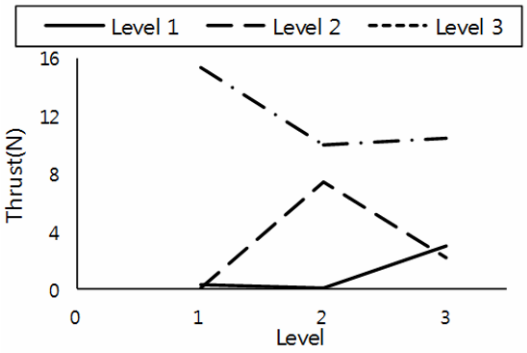

(b) Cross-sectional type

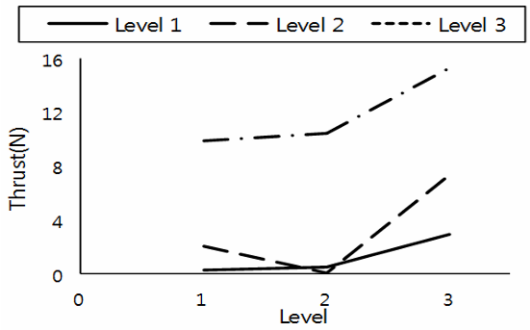

(c) Twist position

Fig. 13. Factor interactions with twist angle.

hovering thrusts between the best DOE and CFD values from the predictive design. The cyclic value of two maximum thrust along the azimuth direction shows that thrusts generating from four rotors are relatively stable. It was also confirmed that the predictive design presented a larger thrust than the best in DOE #8.

6. Concluding remarks

The present study deals with aerodynamic parameter analysis and design of a quad-rotor air vehicle in hover based on Computational fluid dynamics (CFD) and Design of experiments (DOE). This study aimed to obtain the maximum hovering thrust by changing the blade shape without affecting the weight of the quad-copter.

Table 7. Comparison of predictive design and CFD validation.

	Twist [deg]	Max. chord position	Section type	Twist position	Thrust [N]
Best in DOE (#8)	50	r/R = 20 %	Symmetric	r/R = 40 %	15.3068
Predictive design (ANOM)	50	r/R = 30 %	NACA0012	r/R = 40 %	16.0069
CFD validation					15.7337

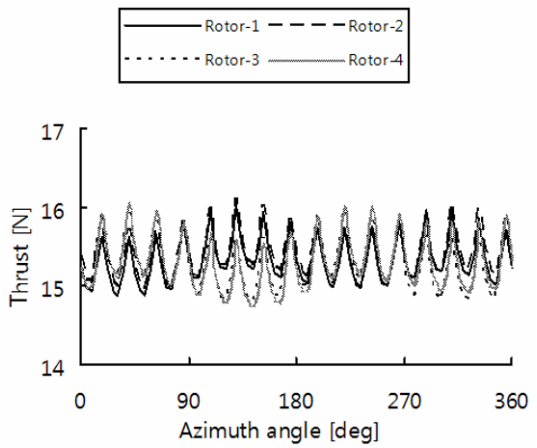

(a) Best in orthogonal array (DOE #8 in Table 5)

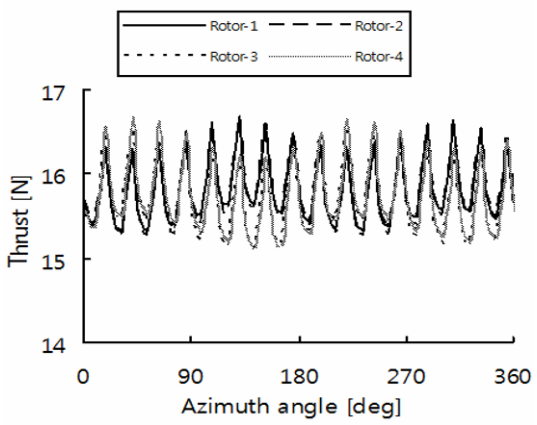

(b) Predictive design with ANOM

Fig. 14. Comparison of hovering thrust with optimized blade shape parameters.

The effect of the rotor-to-rotor distance was analyzed by considering the aerodynamic interference effect as a function of Center distance (CD); the flow interference was detected according to the center distance between rotors under the rotating flow. By selecting three conditions (CD = 300 mm, 400 mm and 500 mm) for the distance between rotors and a rotational speed of 5200 rpm, the interference effect was analyzed as a function of the distance between rotors. Finally, the thrust performance based on blade shape was analyzed by selecting CD = 400 mm for the distance between rotors in a quad-copter.

The factors and levels of the blade shape changes were selected and used in the DOE, and the thrust values were calculated. Afterwards, the factors affecting the hovering thrust were identified through the Analysis of means (ANOM). The blade-shape parameter values that produced the maximum thrust performance were identified through a predictive equation, by which the blade shape of the optimal level combination was derived. Among the factors affecting the hovering thrust, the twist angle and starting position of the twist angle caused the largest contribution in the thrust performance. In addition, actual flow computation was conducted to show that similar values were observed when modeling of the combination was performed for the levels of factors obtained with the predictive equation.

For additional research in this context, aerodynamic performance evaluation in forward flight and robust design under wind and weather conditions should be conducted.

Acknowledgment

This work was supported by the Korea Institute of Energy Technology Evaluation and Planning (KETEP) and the Ministry of Trade, Industry & Energy (MOTIE) of Republic of Korea (No. 20163030024420).

Nomenclature

T : Thrust
b : Number of blades
c : Chord length
V_r : Induced velocity
Ω : Rotational speed
r : Radial direction length of blade
C_L : Lift coefficient
α : Angle of attack
Re : Reynolds number
ρ : Density
μ : Viscosity
$\vec{V}_t$: Linear velocity
$\vec{\omega}$: Angular velocity
$\vec{r}_o$: Position vector
$\vec{v}_r$: Relative velocity (The velocity viewed from the moving frame)
$\vec{v}$: Absolute velocity (The velocity viewed from the stationary frame)
$\vec{u}_r$: Velocity of the moving frame (Relative to the inertial reference frame)
$\vec{V}_t$: Translational frame velocity
$\vec{\tau}$: Viscous stress
E_r : Internal energy
H_r : Total energy
$\vec{F}$: Applied loads

ψ : Azimuth angle dependent on rotational direction
R_0 : Initial position of blade
R_1 : End position of blade

References

[1] A. R. Girard, A. S. Howell and J. K. Hedrick, Border patrol and surveillance missions using multiple unmanned air vehicles, *Proceedings of the 43rd IEEE Conference on Decision and Control*, 1 (2004) 620-625.

[2] A. Le Pape and P. Beaumier, Numerical optimization of helicopter rotor aerodynamic performance in hover, *Aerospace Science and Technology*, 9 (3) (2005) 191-201.

[3] J. H. Yun, H.-Y. Choi and J. Lee, CFD-based thrust analysis of unmanned aerial vehicle in hover mode: Effects of single rotor blade shape, *Transactions of the Korean Society of Mechanical Engineers A*, 38 (5) (2014) 513-520.

[4] P. Pounds, R. Mahony, J. Gresham, P. Corke and J. Roberts, Towards dynamically-favourable quad-rotor aerial robots, *Proceedings of the 2004 Australasian Conference on Robotics & Automation*, Canberra, Australia, April (2004).

[5] H. Huang, G. M. Hoffmann, S. L. Waslander and C. J. Tomlin, Aerodynamics and control of autonomous quadrotor helicopters in aggressive maneuvering, *Proceedings of International Conference on Robotics and Automation 2009*, Kobe, Japan, May (2009) 3277-3282.

[6] E. Çetinsoy, S. Dikyar, C. Hançer, K. T. Oner, E. Sirimoglu, M. Unel and M. F. Aksit, Design and construction of a novel quad tilt-wing UAV, *Mechatronics*, 22 (6) (2012) 723-745.

[7] S. U. Islam, C. Y. Zhou and F. Ahmad, Numerical simulations of cross-flow around four square cylinders in an in-line rectangular configuration, *World Academy of Sciences, Engineering Technology*, 33 (2009) 824-833.

[8] D. Aleksandrov and I. Penkov, Optimization of lift force of mini quad rotor helicopter by changing of distance size between rotors, *Solid State Phenomena*, 198 (2013) 226-231.

[9] Y. Naidoo, R. Stopforth and G. Bright, Quad-rotor unmanned aerial vehicle helicopter modelling & control, *International Journal of Advanced Robotic System*, 8 (4) (2011) 139-149.

[10] P. C. Trizaila, Aerodynamics of low Reynolds number rigid flapping wing under hover and free-stream conditions, *Ph.D. Dissertation*, Department of Aerospace Engineering, The University of Michigan (2011).

[11] V. K. Lakshminarayan and J. D. Baeder, Computational investigation of micro hovering rotor aerodynamics, *Journal of the American Helicopter Society*, 55 (2) (2010) 22001.

[12] *ANSYS FLUENT 14.5 Help*, ANSYS, INC., Canonsburg, PA (2013).

[13] T. H. Kim, S. J. An, Y. D. Jo, K. M. Moon, B. Y. Bae and D. H. Yang, A study on the composite blade performance variation by attaching erosion shield for hovercraft, *Journal of the Korean Society of Marine Engineering*, 33 (7) 1017-1025.

[14] R. Steij and G. Barakos, CFD analysis of rotor-fuselage interactional aerodynamics, *Proceedings of the 45th AIAA Aerospace Sciences Meeting and Exhibit*, Reno, NV, January (2007).

[15] M. H. Mohamed, A. M. Ali and A. A. Hafiz, CFD analysis for H-rotor darrieus turbine as a low speed wind energy converter, *International Journal of Engineering Science and Technology*, 18 (1) (2014) 1-13.

[16] S. W. Lee and O. J. Kwon, Aerodynamic shape optimization of hovering rotor blades in transonic flow using unstructured meshes, *AIAA Journal*, 44 (8) (2006) 1816-1825.

[17] W. Y. Fowlkes and C. M. Creveling, *Engineering methods for robust product design*, Addison Wesley, Reading, MA (1995).

Jongsoo Lee received B.S. in Mechanical Engineering at Yonsei University, Korea in 1988 and Ph.D. in Mechanical Engineering at Rensselaer Polytechnic Institute, Troy, NY in 1996. After a Research Associate at Rensselaer Rotorcraft Technology Center, he is a Professor of Mechanical Engineering at Yonsei University. His research interests include multi-disciplinary/multi-physics/multi-scale design optimization and reliability-based robust engineering design with applications to structures, structural dynamics, fluid-structure interactions and flow induced noise and vibration problems.

Jaehyun Yoon is a Ph.D. student in Mechanical Engineering at Yonsei University. His research interests are on the Aerodynamics, Dynamics, Control and Optimization in Robust Design of Multi-Rotor Air Vehicles.